



OPEN ACCESS

EDITED BY

Daniilo Manzani,
University of São Paulo, Brazil

REVIEWED BY

Nagia S. Tagiara,
National Hellenic Research Foundation,
Greece

Acácio Andrade,
Federal University of Uberlandia, Brazil

*CORRESPONDENCE

M. A. M. Uosif,
✉ Mauosif@ju.edu.sa
Antoaneta Ene,
✉ antoaneta.ene@ugal.ro
Shams A. M. Issa,
✉ shams_issa@yahoo.com
Hesham M. H. Zakaly,
✉ h.m.zakaly@gmail.com

[†]The work of the author AE and APC was covered by "Dunarea de Jos" University of Galati, Romania

RECEIVED 22 April 2023

ACCEPTED 31 May 2023

PUBLISHED 20 June 2023

CITATION

Uosif MAM, Issa SAM, Ene A, Mostafa AMA, Atta A, Badawi A, El Agammy EF and Zakaly HMH (2023), A promising alternative: examining TVS tellurite glass for gamma radiation shielding applications. *Front. Mater.* 10:1210524. doi: 10.3389/fmats.2023.1210524

COPYRIGHT

© 2023 Uosif, Issa, Ene, Mostafa, Atta, Badawi, El Agammy and Zakaly. This is an open-access article distributed under the terms of the [Creative Commons Attribution License \(CC BY\)](https://creativecommons.org/licenses/by/4.0/). The use, distribution or reproduction in other forums is permitted, provided the original author(s) and the copyright owner(s) are credited and that the original publication in this journal is cited, in accordance with accepted academic practice. No use, distribution or reproduction is permitted which does not comply with these terms.

A promising alternative: examining TVS tellurite glass for gamma radiation shielding applications

M. A. M. Uosif^{1*}, Shams A. M. Issa^{2,3*}, Antoaneta Ene^{4*†}, A. M. A. Mostafa¹, Ali Atta¹, Ali Badawi⁵, E. F. El Agammy¹ and Hesham M. H. Zakaly^{2,6,7*}

¹Physics Department, College of Science, Jouf University, Sakaka, Saudi Arabia, ²Department of Physics, Faculty of Science, University of Tabuk, Tabuk, Saudi Arabia, ³Physics Department, Faculty of Science, Al-Azhar University, Assiut, Egypt, ⁴INPOLDE Research Center, Department of Chemistry, Physics and Environment, Faculty of Sciences and Environment, Dunarea de Jos University of Galati, Galati, Romania, ⁵Department of Physics, College of Science, Taif University, Taif, Saudi Arabia, ⁶Computer Engineering Department, Faculty of Engineering and Natural Sciences, Istinye University, Istanbul, Türkiye, ⁷Institute of Physics and Technology, Ural Federal University, Yekaterinburg, Russia

Radiation shielding is crucial in many types of medical, industrial, and nuclear facilities due to the widespread usage of radioactive isotopes. In this research, we examine the impact of tellurite $65\text{TeO}_2-(35-x)\text{V}_2\text{O}_5-x\text{Sm}_2\text{O}_3$ glasses, where x ranges from 0.1 to 5 mol%, for its nuclear security and radiation shielding *versus* gamma attenuation capabilities. For gamma, the effect that the systematic replacement of Sm_2O_3 with V_2O_5 has on the shielding qualities was dissected in great depth. In addition, comparative research was carried out using the most recent borate glasses and the typical shielding materials considered the industry standard. In this study, we utilized the FLUKA algorithm and the FLAIR graphical interface to calculate the attenuation coefficients of glass compositions in the $65\text{TeO}_2-(35-x)\text{V}_2\text{O}_5-x\text{Sm}_2\text{O}_3$ system. The gamma energies of 0.356, 0.662, 1.332, and 2.614 MeV, commonly used in gamma shielding investigations, were selected as the radiation source. A comparison between the simulation results by FLUKA and theoretical calculations for mass attenuation coefficients demonstrated excellent agreement, confirming the reliability and accuracy of the FLUKA simulation method. The findings of the current research point to the fact that the TVS5 sample has the highest G_{MAC} and lowest G_{HVL} and G_{MFP} , among other glasses. This points to the possibility that the TVS5 sample might be used in radiation shielding activities, which would result in increased nuclear safety.

KEYWORDS

tellurite glass, gamma radiation, FLUKA, Sm_2O_3 , tellurite glass, gamma radiation, Sm_2O_3

1 Introduction

Radioactive isotopes and the technologies involved with nuclear radiation play a major part in the contemporary existence of humans. Isotopes are a naturally occurring source of radiation, and as such, they have a wide range of uses. One of these applications is excellent tracers owing to the fact that their radioactivity can be readily identified. Isotopes are used to eliminate germs and viruses that may be present in food by harnessing the energy that they produce (sterilize foodstuffs). In addition to this,

radioactive isotopes have a wide variety of uses in the field of medicine. One example of this would be the use of radioactive ¹³¹I in a diagnostic setting to evaluate thyroid function (Ladenson et al., 1997). In addition, ²²Na is used in the field of nuclear scanning because of the novel chemical characteristics it has. There are various applications for several radioactive isotopes, such as ¹³¹I and ²²Na, in a wide range of industry applications, covering agricultural production and virtually entirely all nuclear plants (Schellekens et al., 2011; Hussey et al., 2012).

It has been discovered that unintended exposure to the radiation, that is, released by radioactive isotopes may have a harmful impact on both living creatures and the environment. This is the case even though radioactive isotopes have a wide range of uses. The kind and quantity of energy that isotopes of radioactive substances release into the environment determine the degree of danger they pose. For instance, excessive dosages may result in cataracts, damage to DNA, infertility, cancer, and a variety of blood-related illnesses (Miousse et al., 2017; Elazaka et al., 2021). The use of shielding materials is encouraged, particularly for personnel who often interact with radioactive substances, whether at a clinic or other nuclear facility, to reduce the chance of a situation like this occurring. As a result, the reduction of radiation exposure for both humans and the environment should be one of the primary goals of utilizing a shielding material (Al-Hadeethi et al., 2020; Mahmoud et al., 2021). Due to the high atomic numbers of its elements and the high density of lead, concrete and lead compounds have been more popular over the years as trustworthy materials for use in nuclear security applications. Nevertheless, the use of lead materials is subject to various regulations and major problems (such as toxicity), which must be considered. This incentivises scientists to continue their search for a novel material that may be used to guard *versus* radiation (Rammah et al., 2020; El-Denglawey et al., 2021; Kilic et al., 2021). In this context, glass systems are intriguing options owing to their benefits compared to other materials such as metal alloys, polymers, and opaque materials. In a nutshell, the easiest fabrication techniques, the lowest cost, the capacity to be recycled, and the transparency to light are the characteristics of the glasses that are considered the most significant (Susoy et al., 2020; Zakaly et al., 2021b; Zakaly et al., 2021a).

Glasses made of oxides are used extensively in a variety of commercial, technical, and industrial settings. These glasses have several unique characteristics, such as high density, high refractive index, great thermal expansion, and low transition temperatures. In addition, they have excellent chemical endurance (Al-Hadeethi and Sayyed, 2020; Ilik et al., 2022). On the other hand, metal oxides such as TeO₂ and Sm₂O₃, which have a high atomic number (Z) as well as a high density, have the potential to be researched for use in radiation shielding technologies. In fact, the capability of the material to deflect radiation is enhanced as its Z rises. This is because an increased number of atoms results in an increased number of atoms that can interact with radiation photons (D'Souza et al., 2020; Saudi et al., 2021). TeO₂ glasses are compounds that are viewed as having potential for several optical applications as well as applications requiring radiation shielding. This is due to the extraordinary qualities that TeO₂ glasses possess. Recent studies have demonstrated that TeO₂

TABLE 1 Elemental compositions of glasses.

Code	TeO ₂	V2O5	Sm ₂ O ₃	Te	O	V	Sm
TVS0.1	61.91	37.88	0.21	0.4950	0.2910	0.2122	0.0018
TVS0.5	61.66	37.30	1.04	0.4930	0.2891	0.2089	0.0089
TVS1	61.36	36.58	2.06	0.4906	0.2867	0.2049	0.0178
TVS2	60.76	35.15	4.08	0.4858	0.2821	0.1969	0.0352
TVS3	60.17	33.76	6.07	0.4811	0.2775	0.1891	0.0523
TVS4	59.60	32.39	8.01	0.4765	0.2730	0.1814	0.0691
TVS5	59.03	31.05	9.92	0.4719	0.2686	0.1739	0.0856

glasses have significant shielding capabilities that are either on par with or even better than those afforded by other kinds of glass systems (Almuqrin et al., 2021). The ability to employ tellurite-based glasses in a radiation-contaminated environment depends critically on understanding their shielding efficacy and ability to reduce radiation exposure severity (Çelikbilek et al., 2013). In recent years, among various kinds of composite, samarium glasses have been very influential to scientists, particularly for studies on excited state absorption, laser characteristics, and spectral hole burning.

The focus of the current research report is the influence of the network modifier Sm_2O_3 content on the radiation shielding properties of Sm^{3+} -doped tellurite glasses. Because of its expansive glass forming range, which may range from 0.1 to 5 mol%, tellurite glass is an appealing technology. This is because the network modifier content can change within this range. The radiation shielding characteristics of tellurite inside the network may also be influenced by the network modifier Sm_2O_3 . Sm_2O_3 is an effective radiation shield that may be used to protect against high-energy nuclear radiation.

Optical and luminescence properties of Sm_2O_3 doped $\text{SrO-PbO-ZnO-P}_2\text{O}_5\text{-TeO}_2$ glasses for visible laser applications were studied by Biswas et al. (2022). Gamma-ray shielding properties of $\text{TeO}_2\text{-ZnF}_2\text{-As}_2\text{O}_3\text{-Sm}_2\text{O}_3$ glasses have been investigated by Gaikwad et al. (2018). UV and electrical properties of $\text{TeO}_2\text{-WO}_3\text{-Li}_2\text{O-Nb}_2\text{O}_5/\text{Sm}_2\text{O}_3/\text{Pr}_6\text{O}_{11}/\text{Er}_2\text{O}_3$ glasses have been examined by Ibrahim et al. (2018). Selvi et al. (2017) studied the Effect of PbO on the $\text{B}_2\text{O}_3\text{-TeO}_2\text{-P}_2\text{O}_5\text{-BaO-CdO-Sm}_2\text{O}_3$ glasses—Structural and optical investigations. Divina et al. (2019) recorded the Physical, structural, and radiation shielding properties of the $\text{B}_2\text{O}_3\text{-MgO-K}_2\text{O-Sm}_2\text{O}_3$ glass network modified with TeO_2 . The correlation between the concentration of TeO_2 and the radiation shielding properties in the $\text{TeO}_2\text{-MoO}_3\text{-V}_2\text{O}_5$ glass system has been studied by Al-Hadeethi and Sayyed (2023). Gamma and neutron shielding characterizations of the $\text{Ag}_2\text{O-V}_2\text{O}_5\text{-MoO}_3\text{-TeO}_2$ quaternary tellurite glass system with the Geant4 simulation toolkit and Phy-X software has been recorded by Aşkın (2020). The main goal of the current research article is to analyze the gamma attenuation characteristics of the $65\text{TeO}_2\text{-(35-x)V}_2\text{O}_5\text{-xSm}_2\text{O}_3$ glass system for energy levels between 0.015 and 15 MeV. The data acquired from the current investigation is intended to add to the literature, notably in terms of monitoring the impacts of Sm_2O_3 contribution on TeO_2 glasses.

2 Materials and methods

In a crucible that was covered, TeO_2 , V_2O_5 , and Sm_2O_3 oxide were mixed in particular proportions to produce tellurite glass, which was then used to make glass samples. The mixture was maintained at a temperature of 300°C for 1 h in order to limit the propensity toward volatilization. After that, the porcelain crucible was moved to a muffle furnace, which had its temperature set anywhere between 720°C and 750°C , depending on the nature of the material being tested. The crucible remained in the furnace for a period of 30 m. After pouring the molten metal into a steel mold at ambient temperature, it was then annealed at a

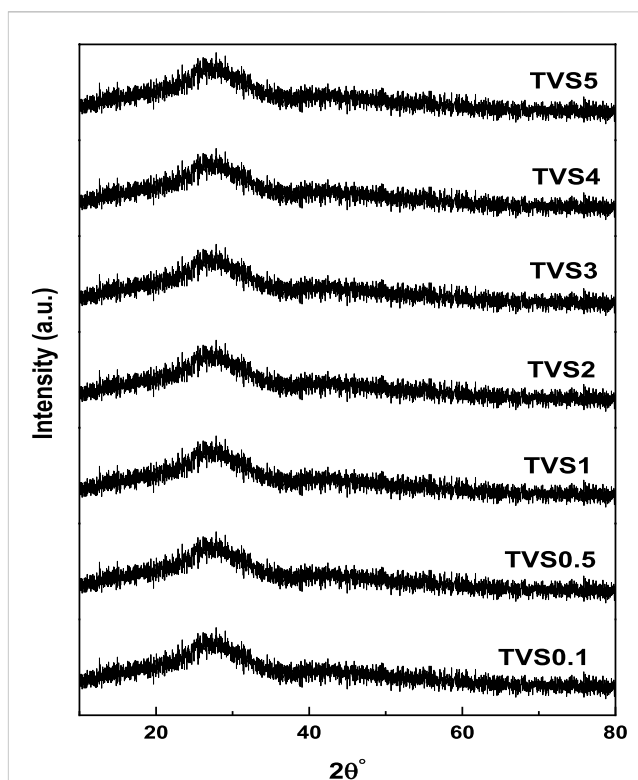


FIGURE 1
XRD profiles of powder TVS0.1 and TVS5 glasses.

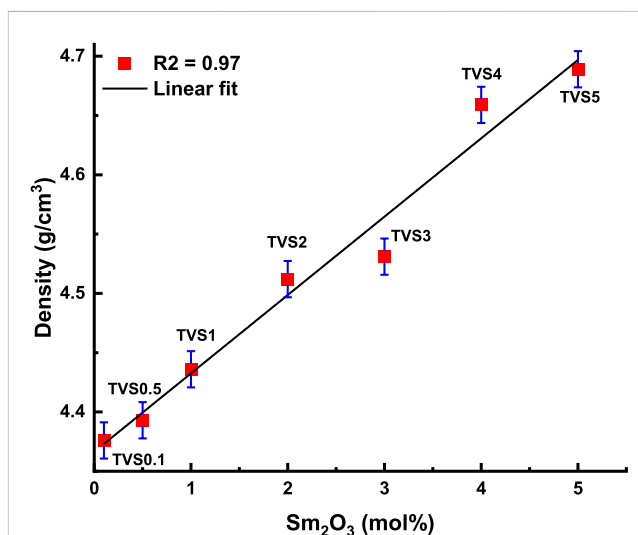


FIGURE 2
Dependence of bulk density on Sm_2O_3 mol% content in glasses.

temperature of 300°C for 1 h. Polishing was performed on two sides of each glass sample opposite to one another to achieve optically flat and parallel faces (Table 1) (Sidkey et al., 1999). By using the displacement technique with $\text{C}_6\text{H}_5\text{CH}_3$ as the immerse solvent, the density of the glass samples could be determined with an accuracy of up to the third decimal place. Examination by X-ray diffraction was performed using a Philips PW/1710 equipped with a

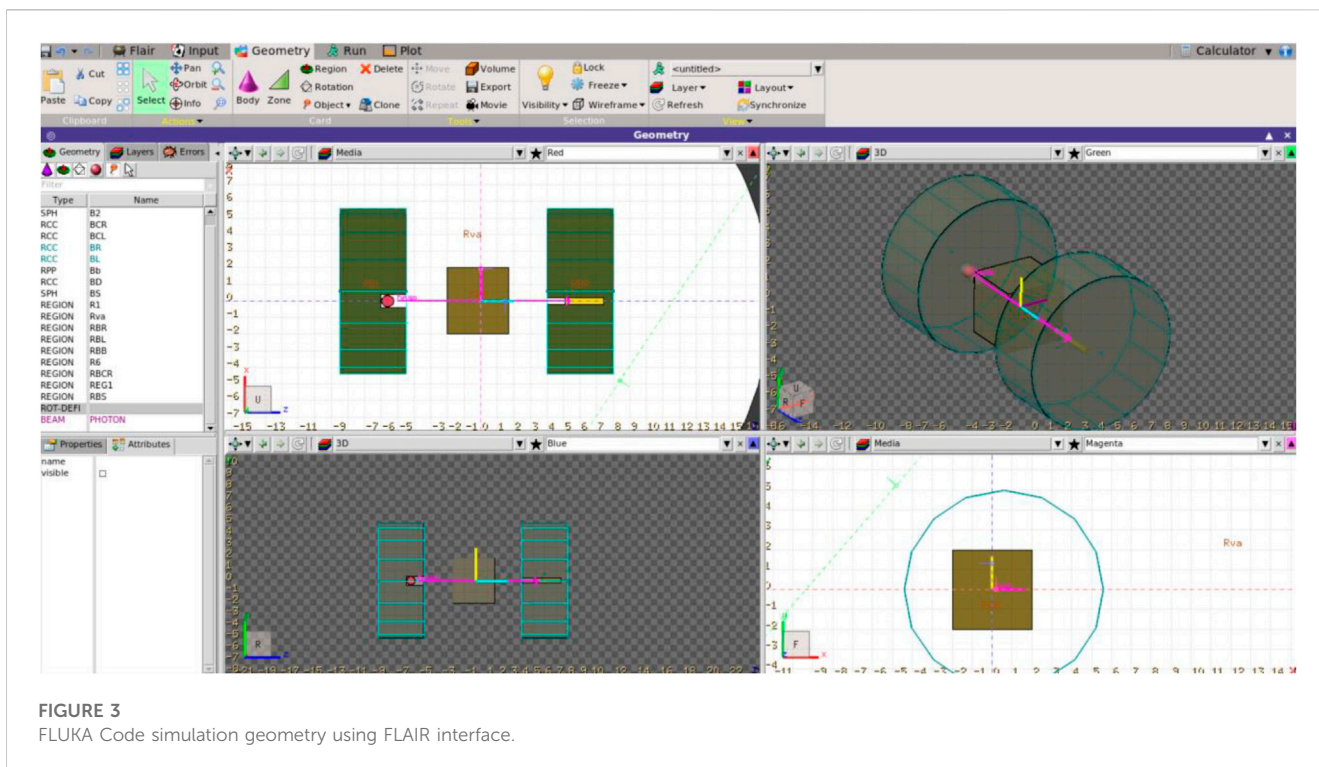


FIGURE 3 FLUKA Code simulation geometry using FLAIR interface.

Ni-filter, Cu radiation at 40 kV and 30 mA; these settings were maintained throughout the process. The mass attenuation coefficient (G_{MAC}) for these glasses was determined with the use of the Phy-X program (Şakar et al., 2020), which covered the energy range of 0.015–15 MeV. The G_{MAC} allows us to investigate the effect that the concentrations of Sm_2O_3 have on the glasses' ability to attenuate sound. In addition, the breadth of the material that has the potential to block fifty percent of the initial photons is referred to as the half-value layer (G_{HVL}) (Mostafa et al., 2020a; Sadeq et al., 2022).

3 Results and discussions

The XRD spectra of the TVS0.1, TVS0.5, TVS1, TVS2, TVS3, TVS4, and TVS5 glasses are presented in Figure 1. The diffraction patterns of the glasses show broad peaks, which are typical of fully amorphous material and no sharp peaks were observed that would indicate signs of crystallization. The density (ρ) of a material is one of the commonly recognized descriptive tools that have been utilized for a long time and is dependent on the change in the atomic mass as well as the spatial organization of the material's bulk. As can be seen in Figure 2, the addition of Sm_2O_3 resulted in a significant shift in the density readings taken from the samples now being examined (Turky and Dawy, 2003). The ρ that was examined was found to rise from 4.367 (g/cm^3) for a TVS0.1 sample (lowest Sm_2O_3 content) to 4.598 (g/cm^3) for the sample that had the maximum amount of Sm_2O_3 . This observed rise is connected to the influence of the molecule's molecular weight. The incorporation of Sm_2O_3 with a high molecular weight (348.72 g/mol) and a high density (8.347 g/cm^3), at the cost of V_2O_5 , which has a low molecular weight (181.88 g/mol) and a low density (3.357 g/cm^3). This data substantiates the hypothesis that the addition of Sm_2O_3 causes a

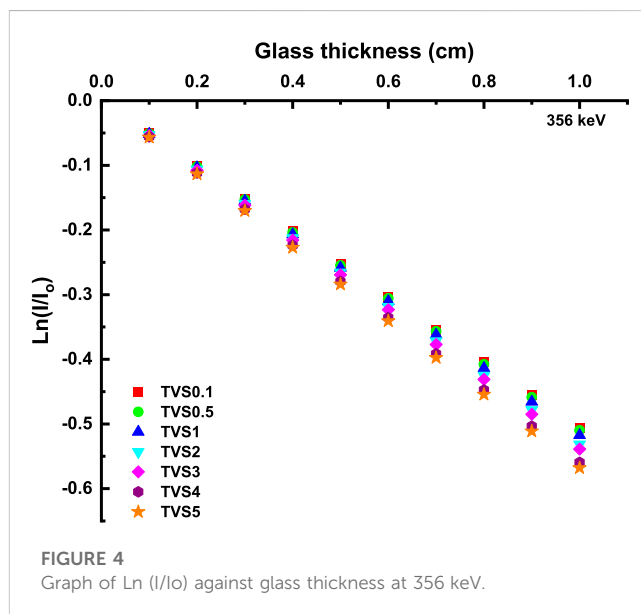


FIGURE 4 Graph of $\ln(I/I_0)$ against glass thickness at 356 keV.

dense crowding of the glass network. The same effect was seen in the borate after it had been doped with heavy metal oxide in the referenced study (Sidkey et al., 1999).

3.1 FLUKA Monte Carlo simulation

The FLUKA (FLUKtuierende KASKade in German, signifying fluctuating cascade) is a versatile Monte Carlo code widely employed in various physics research domains, including nuclear, accelerator,

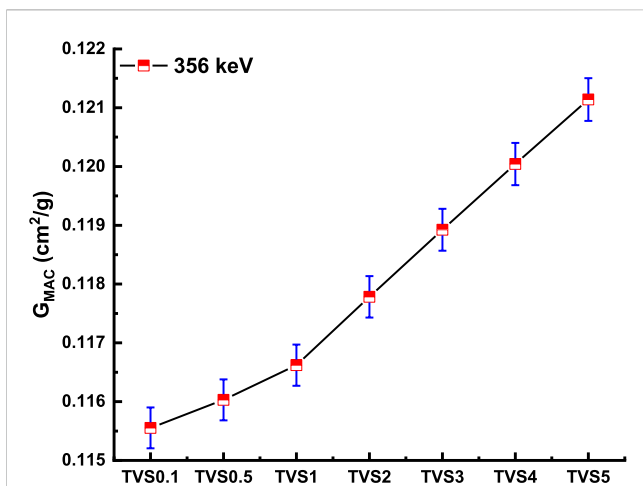


FIGURE 5
Dependence of mass attenuation coefficient (G_{MAC}) on Sm_2O_3 mol% content in glasses.

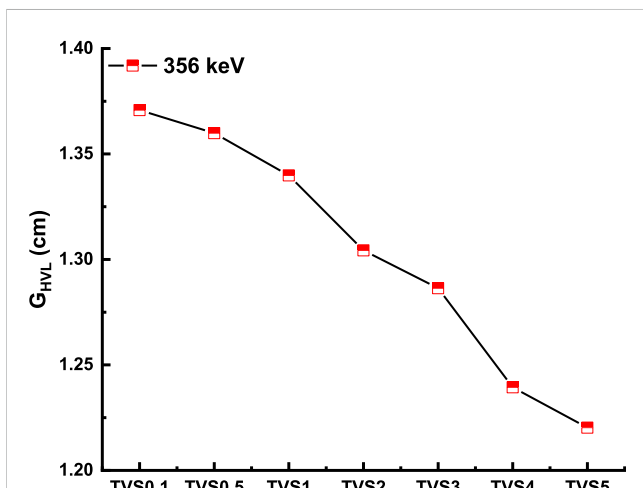


FIGURE 6
Dependence of half value layer (G_{HVL}) on Sm_2O_3 mol% content in glasses.

high energy, and particle physics (Ferrari et al., 2005; Battistoni et al., 2007; Mostafa et al., 2020b). A distinguishing feature of FLUKA compared to other Monte Carlo codes is its ability to operate in both adjustable and analogue modes. The Flair graphical interface, extensively used for radiobiological effect analysis, is incorporated in the current version (accessible at <http://flair.cern>), which introduces novel features such as advanced 3D visualization with photorealistic rendering and support for industry-standard volume depiction of medical phantoms.

FLUKA has been instrumental in determining radiation conditions for electronic components, assessing their reactions to diverse scenarios not covered by radiation testing regulations for space and accelerators, and beyond the scope of traditional ground-level testing. Users must provide the geometry, material, source properties, and scoring type for a specific problem using commands known as cards in a standard FLUKA

input file (Mark et al., 2007; Rashad et al., 2020; Zakaly et al., 2022). The FLAIR graphical interface was employed to construct the input file necessary for calculating the mass attenuation coefficients of glass compositions in the $65TeO_2-(35-x)V_2O_5-xSm_2O_3$ system, where x ranges from 0.1 to 5 mol%, using the FLUKA algorithm (Figure 3). The DEFAULTS card in the input file is configured to EM-CASCADE, specifying FLUKA defaults for a particular problem type, and enabling electromagnetic interactions, Rayleigh scattering, and Compton scattering. Gamma energies of 0.356, 0.662, 1.332, and 2.614 MeV, commonly used in gamma shielding studies, were selected as the radiation source, oriented along the z-axis.

Table 1 presents the atomic number, mass number, and densities of the glass samples' elemental composition, determined using elemental mass fraction characteristics. Figure 3 illustrates the precise design of the geometry created for the FLUKA method, the body and region used in the simulation geometry, and a snapshot of the side, top, front, and rear views in the FLAIR geometry editor (Madbouly et al., 2022; Zhukovsky et al., 2022). The glass sample geometry was designed as a 5 cm radius circular cylinder parallel to the z-axis, segmented into various thicknesses using XYP planes (bounded by a plane perpendicular to the z-axis) (El-Taher et al., 2021).

3.2 Mass attenuation coefficient (G_{MAC})

After calculating the linear attenuation coefficient (G_{LAC}) by first measuring the intensities of the gamma rays that were incident (I_0) and transmitted (I), the resultant value was used to calculate the G_{MAC} . To get the values of the G_{LAC} , one must first calculate the slope of the linear graph that plots $\ln(I/I_0)$ versus the specimen thickness. Figure 4 depicts $\ln(I/I_0)$ vs. the sample thickness for all glasses measured at 356 keV; The patterns are almost identical for each and every photon energy. As additional Sm_2O_3 is added, the slope of the graph goes up, as can be seen in Figure 4. This happens on average. When the amount of Sm_2O_3 in the sample increases from 0.1 to 5 mol%, the slope of the graph increases from 0.506 to 0.568 at 356 keV (an example). The Glass in this specific set of glasses had the biggest gradient in the Glass with the highest concentration of Sm_2O_3 , which may be interpreted as having the highest values of G_{LAC} in contrast to other glasses.

Take notice that the Z of Sm is 62, which is a much greater figure than the one for V (23). If a high percentage of Sm is included into the composition of the Glass, the gamma will be subjected to a more robust level of interaction with the Sm atoms that make up the Glass. Before an electron can be released from an Sm atom, a bigger quantity of photon energy must be absorbed. This is because the higher the Z, the more energy there is to absorb. It's possible that the electron was ejected due to either the photoelectric effect (PE) or the Compton scattering (CS), but it was not both. The quantity of gamma rays that can pass through the Glass is reduced when there is a higher degree of interaction between the gamma and the target atom (Sm). This was a direct contributor to the increase in the G_{MAC} that occurred (Issa and Mostafa, 2017). The addition of the modulator to the Glass is another factor that led to the growth in the value of the G_{MAC} . It is believed that lowering the porosity nature of the Glass and generating high Glass can be accomplished by adding a high modifier ($Sm_2O_3 = 8.347 \text{ g/cm}^3$) into the glass system. This is because large modifiers have a greater surface area than low

TABLE 2 Mass attenuation coefficient at selected photon energy for all glasses.

E (MeV)	TVS0.1	TVS0.5	TVS1	TVS2	TVS3	TVS4	TVS5
1.50E-02	34.272	34.655	35.130	36.066	36.984	37.884	38.768
2.00E-02	15.663	15.845	16.071	16.516	16.952	17.380	17.799
3.00E-02	5.215	5.278	5.356	5.511	5.662	5.810	5.956
4.00E-02	10.831	10.827	10.822	10.813	10.805	10.796	10.788
5.00E-02	6.047	6.147	6.270	6.513	6.751	6.984	7.214
6.00E-02	3.739	3.801	3.878	4.030	4.179	4.325	4.468
8.00E-02	1.762	1.791	1.827	1.898	1.968	2.036	2.103
1.00E-01	1.003	1.019	1.039	1.077	1.116	1.153	1.190
1.50E-01	0.399	0.404	0.410	0.423	0.436	0.448	0.460
2.00E-01	0.235	0.237	0.240	0.246	0.251	0.257	0.262
2.23E-01	0.198	0.199	0.202	0.206	0.210	0.214	0.218
2.76E-01	0.150	0.151	0.152	0.154	0.156	0.159	0.161
2.84E-01	0.145	0.146	0.147	0.150	0.152	0.154	0.156
3.00E-01	0.137	0.137	0.138	0.140	0.142	0.144	0.146
3.03E-01	0.135	0.136	0.137	0.139	0.140	0.142	0.144
3.47E-01	0.118	0.119	0.119	0.121	0.122	0.123	0.124
3.56E-01	0.116	0.116	0.117	0.118	0.119	0.120	0.121
3.84E-01	0.108	0.109	0.109	0.110	0.111	0.112	0.113
4.00E-01	0.105	0.105	0.105	0.106	0.107	0.108	0.109
5.00E-01	0.089	0.089	0.089	0.090	0.090	0.091	0.091
6.00E-01	0.079	0.079	0.079	0.080	0.080	0.080	0.080
6.62E-01	0.075	0.075	0.075	0.075	0.075	0.075	0.075
8.00E-01	0.067	0.067	0.067	0.067	0.067	0.067	0.067
8.26E-01	0.066	0.066	0.066	0.066	0.066	0.066	0.066
1.00E+00	0.059	0.059	0.059	0.059	0.059	0.059	0.059
1.17E+00	0.054	0.054	0.054	0.054	0.054	0.054	0.054
1.33E+00	0.050	0.050	0.050	0.050	0.050	0.050	0.050
1.50E+00	0.048	0.048	0.048	0.048	0.048	0.048	0.048
2.00E+00	0.042	0.042	0.042	0.042	0.042	0.042	0.042
2.51E+00	0.038	0.038	0.038	0.038	0.038	0.038	0.038
3.00E+00	0.036	0.036	0.036	0.036	0.036	0.036	0.036
4.00E+00	0.033	0.033	0.033	0.033	0.033	0.033	0.034
5.00E+00	0.032	0.032	0.032	0.032	0.032	0.032	0.032
6.00E+00	0.031	0.031	0.031	0.031	0.032	0.032	0.032
8.00E+00	0.031	0.031	0.031	0.031	0.031	0.032	0.032
1.00E+01	0.031	0.031	0.031	0.032	0.032	0.032	0.032
1.50E+01	0.033	0.033	0.033	0.033	0.034	0.034	0.034

TABLE 3 Half value layer at selected photon energy for all glasses.

E (MeV)	TVS0.1	TVS0.5	TVS1	TVS2	TVS3	TVS4	TVS5
1.50E-02	0.005	0.005	0.004	0.004	0.004	0.004	0.004
2.00E-02	0.010	0.010	0.010	0.009	0.009	0.009	0.008
3.00E-02	0.030	0.030	0.029	0.028	0.027	0.026	0.025
4.00E-02	0.015	0.015	0.014	0.014	0.014	0.014	0.014
4.96E-02	0.026	0.025	0.024	0.023	0.022	0.021	0.020
5.00E-02	0.026	0.026	0.025	0.024	0.023	0.021	0.020
6.00E-02	0.042	0.042	0.040	0.038	0.037	0.034	0.033
8.00E-02	0.090	0.088	0.086	0.081	0.078	0.073	0.070
1.00E-01	0.158	0.155	0.150	0.143	0.137	0.129	0.124
1.50E-01	0.397	0.391	0.381	0.363	0.351	0.332	0.321
2.00E-01	0.675	0.666	0.651	0.625	0.609	0.579	0.563
2.23E-01	0.801	0.791	0.775	0.746	0.728	0.695	0.678
2.76E-01	1.059	1.048	1.029	0.997	0.978	0.937	0.918
2.84E-01	1.090	1.079	1.060	1.027	1.008	0.967	0.948
3.00E-01	1.160	1.149	1.130	1.096	1.077	1.035	1.015
3.03E-01	1.172	1.161	1.142	1.108	1.089	1.046	1.027
3.47E-01	1.340	1.329	1.309	1.274	1.255	1.209	1.190
3.56E-01	1.371	1.360	1.340	1.304	1.286	1.239	1.220
3.84E-01	1.463	1.452	1.432	1.396	1.378	1.329	1.311
4.00E-01	1.513	1.502	1.481	1.445	1.428	1.378	1.360
5.00E-01	1.782	1.771	1.750	1.712	1.696	1.642	1.624
6.00E-01	2.003	1.992	1.970	1.930	1.916	1.858	1.841
6.62E-01	2.124	2.114	2.091	2.051	2.037	1.976	1.959
8.00E-01	2.370	2.359	2.335	2.292	2.279	2.214	2.197
8.26E-01	2.413	2.402	2.378	2.335	2.322	2.255	2.238
1.00E+00	2.684	2.673	2.647	2.601	2.588	2.516	2.498
1.17E+00	2.930	2.919	2.890	2.841	2.829	2.751	2.733
1.33E+00	3.137	3.125	3.094	3.042	3.030	2.946	2.928
1.50E+00	3.330	3.317	3.285	3.230	3.217	3.129	3.109
2.00E+00	3.805	3.790	3.753	3.689	3.672	3.570	3.547
2.51E+00	4.167	4.149	4.107	4.034	4.014	3.900	3.872
3.00E+00	4.432	4.412	4.366	4.285	4.261	4.137	4.105
4.00E+00	4.792	4.768	4.715	4.621	4.588	4.450	4.409
5.00E+00	4.994	4.966	4.908	4.805	4.765	4.615	4.567
6.00E+00	5.102	5.071	5.008	4.898	4.852	4.695	4.642
8.00E+00	5.152	5.118	5.050	4.930	4.876	4.711	4.651
1.00E+01	5.097	5.060	4.990	4.866	4.807	4.639	4.574
1.50E+01	4.849	4.810	4.738	4.611	4.546	4.379	4.310

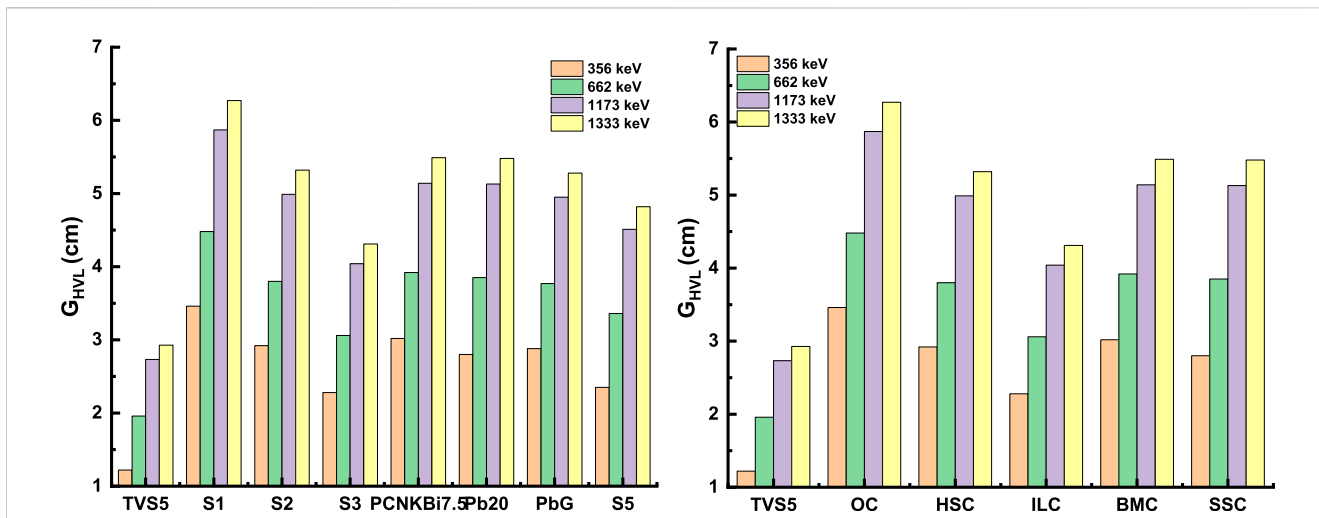


FIGURE 7 The half value layer (G_{HVL}) of the TVS5 glass in comparison to some standard shielding materials and concretes at 356, 662, 1173, and 1333 keV.

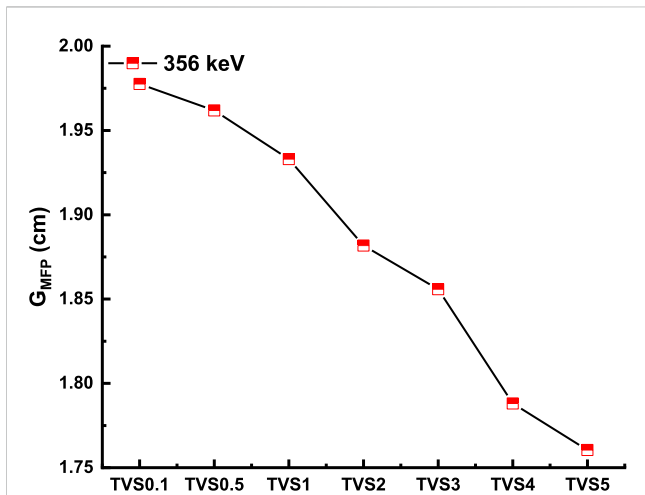


FIGURE 8 Dependence of mean free path (G_{MFP}) on Sm_2O_3 mol% content in glasses.

modifiers. Glass will have a stronger attenuation than other materials because it has a greater potential that gamma rays will interact with the atoms in Glass due to the fact that Glass has a lower porosity than other materials (Bagheri et al., 2017). This is because Glass has a lower porosity than other materials.

The G_{MAC} values for the TVS0.1, TVS0.5, TVS1, TVS2, TVS3, TVS4, and TVS5 samples are shown in Figure 5, at 356 keV; the patterns are almost identical for each photon energy (Table 2). If you look at the graph in Figure 5, you'll see that the values of G_{MAC} increase whenever the concentration of Sm_2O_3 does as well. This is a phenomenon that may be seen for oneself. The $65TeO_2-(35-x)V_2O_5-xSm_2O_3$ glass system has the highest G_{MAC} values, which are respectively $0.121\text{ cm}^2/\text{g}$. This glass system also has the highest G_{MAC} value. As was to be expected based on the predictions, the largest G_{MAC} was produced by the glass system with the maximum

possible concentration of Sm_2O_3 . The higher the G_{MAC} values are, the better a given material is in attenuating a larger number of photons. At the energies that were explored, it was discovered that increasing the quantity of Sm_2O_3 in the glass samples led to an increase in the G_{MAC} . The presence of Sm_2O_3 in these materials causes an increase in both their effective atomic numbers and their densities. This is the rationale for this phenomenon. Compared to other glasses, TVS5 glass ($Sm_2O_3 = 5\text{ mol\%}$) had the highest density, resulting in it having the highest G_{MAC} value. Other glasses were unable to compete with this density. Research demonstrated that the TVS5 glass had the highest possible amount of photon interaction at the energy level that was provided. This interaction could occur as a consequence of the PE, the CS, or the creation of pairs (PP) (Kilic et al., 2020).

3.3 The half value layer (G_{HVL})

How well the glasses protect against G_{HVL} photons is also discussed. It describes the sample thickness at which 50% of the incident radiation intensity is attenuated. In Figure 6, we have a depiction of the TVS0.1, TVS0.5, TVS1, TVS2, TVS3, TVS4, and TVS5 glasses' G_{HVL} at 356 keV. The patterns are almost identical for each photon energy (Table 3). The G_{HVL} varies directly as a function of photon energy (Issa et al., 2020). At 15 keV, the values are at their lowest (between 0.005 and 0.004 cm), while at 15 MeV, they reach their highest (between 4.849 and 4.310 cm). This finding suggests that a very thin layer is required to significantly reduce the intensity of the low-energy photons. Figure 6 demonstrates that there is a direct correlation between a rise in the density of the glasses and a commensurate drop in the G_{HVL} of the samples that were investigated. Because of this pattern in the G_{HVL} , it can be deduced that the TVS5 glass, which is the sample with the highest Sm_2O_3 content and density, is the most effective in blocking photons. The second specimen, TVS0.1, on the other hand, is the one, that is, the least effective in blocking photons because it has the least value and the least quantity of Sm_2O_3 concentration. We are able to provide an explanation for the previously indicated relationship between the G_{HVL} and the density of the TVS0.1, TVS0.5, TVS1, TVS2, TVS3, TVS4, and

TABLE 4 Mean free path at selected photon energy for all glasses.

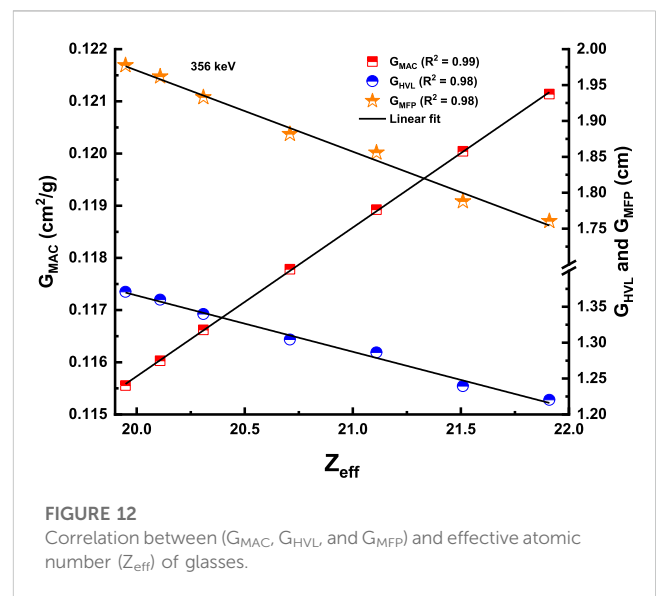
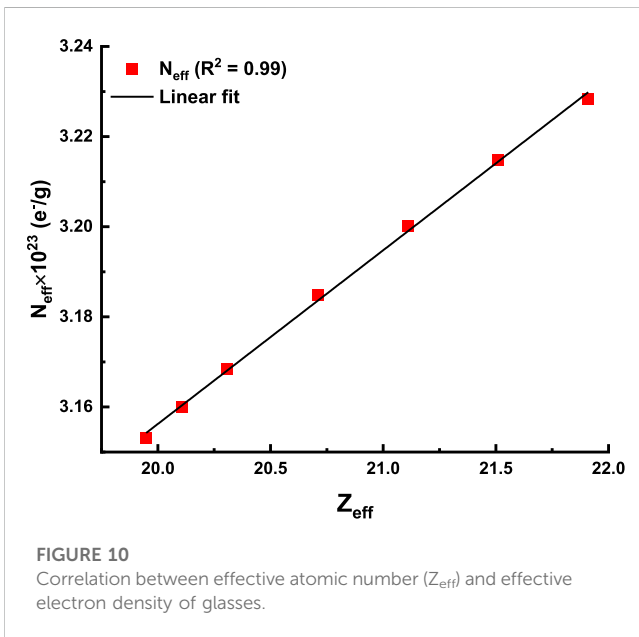
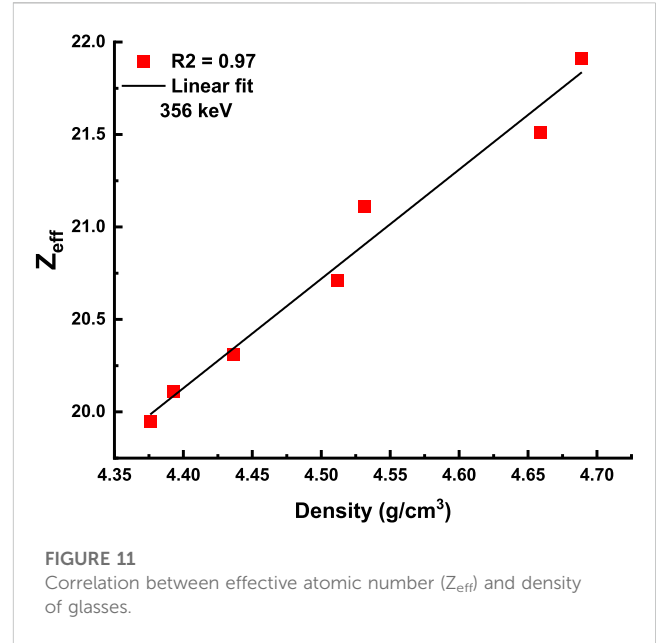
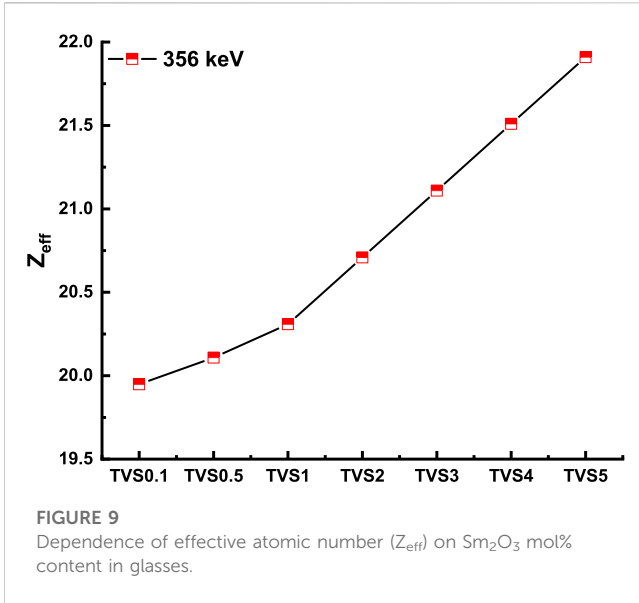
E (MeV)	TVS0.1	TVS0.5	TVS1	TVS2	TVS3	TVS4	TVS5
1.50E-02	0.007	0.007	0.006	0.006	0.006	0.006	0.006
2.00E-02	0.015	0.014	0.014	0.013	0.013	0.012	0.012
3.00E-02	0.044	0.043	0.042	0.040	0.039	0.037	0.036
4.00E-02	0.021	0.021	0.021	0.020	0.020	0.020	0.020
5.00E-02	0.038	0.037	0.036	0.034	0.033	0.031	0.030
6.00E-02	0.061	0.060	0.058	0.055	0.053	0.050	0.048
8.00E-02	0.130	0.127	0.123	0.117	0.112	0.105	0.101
1.00E-01	0.228	0.223	0.217	0.206	0.198	0.186	0.179
1.50E-01	0.573	0.564	0.549	0.524	0.507	0.479	0.463
2.00E-01	0.974	0.961	0.940	0.902	0.878	0.835	0.813
2.84E-01	1.572	1.557	1.530	1.482	1.455	1.395	1.368
3.00E-01	1.673	1.657	1.630	1.581	1.554	1.493	1.465
3.03E-01	1.690	1.675	1.647	1.598	1.571	1.509	1.482
3.47E-01	1.933	1.917	1.888	1.837	1.811	1.744	1.717
3.56E-01	1.978	1.962	1.933	1.882	1.856	1.788	1.760
3.84E-01	2.110	2.095	2.065	2.013	1.988	1.918	1.891
4.00E-01	2.182	2.167	2.137	2.085	2.060	1.988	1.961
5.00E-01	2.570	2.555	2.524	2.469	2.447	2.369	2.343
6.00E-01	2.889	2.874	2.842	2.785	2.765	2.680	2.655
6.62E-01	3.065	3.050	3.016	2.958	2.939	2.851	2.826
8.00E-01	3.419	3.404	3.368	3.307	3.288	3.194	3.169
8.26E-01	3.481	3.466	3.430	3.368	3.350	3.254	3.229
1.00E+00	3.873	3.857	3.818	3.752	3.734	3.629	3.604
1.17E+00	4.228	4.211	4.170	4.099	4.081	3.969	3.943
1.33E+00	4.525	4.508	4.464	4.389	4.371	4.251	4.224
1.50E+00	4.805	4.786	4.740	4.660	4.641	4.514	4.485
2.00E+00	5.490	5.468	5.414	5.321	5.298	5.151	5.117
2.51E+00	6.012	5.986	5.925	5.820	5.791	5.627	5.586
3.00E+00	6.394	6.365	6.298	6.182	6.147	5.969	5.922
4.00E+00	6.914	6.879	6.802	6.667	6.620	6.419	6.361
5.00E+00	7.205	7.165	7.080	6.932	6.874	6.658	6.589
6.00E+00	7.360	7.316	7.225	7.066	7.000	6.773	6.697
8.00E+00	7.433	7.383	7.286	7.113	7.035	6.797	6.710
1.00E+01	7.354	7.301	7.200	7.020	6.935	6.692	6.599
1.50E+01	6.996	6.939	6.836	6.652	6.559	6.318	6.218

TVS5 glasses on the basis of the following: The likelihood of photons interacting with atoms of Glass is very low due to the fact that there is space between the atoms inside the low-density material that gamma rays pass over. As a direct consequence of this, the passage of the

photons through the Glass is made a great deal easier. Because of this, we will need to increase the thickness of the sample in order to absorb the necessary fifty percent of the initial photons. This will lead to a high G_{HVL} for the low-density components. In contrast, there is a good

TABLE 5 Effective atomic number at selected photon energy for all glasses.

E (MeV)	TVS0.1	TVS0.5	TVS1	TVS2	TVS3	TVS4	TVS5
1.50E-02	37.25	37.59	38.01	38.82	39.61	40.38	41.12
2.00E-02	37.42	37.76	38.18	39.00	39.80	40.57	41.32
3.00E-02	37.12	37.47	37.89	38.72	39.52	40.29	41.04
4.00E-02	47.31	47.39	47.49	47.68	47.88	48.07	48.26
5.00E-02	46.63	46.90	47.23	47.85	48.43	48.98	49.49
6.00E-02	45.57	45.85	46.20	46.86	47.47	48.05	48.59
8.00E-02	42.69	43.01	43.39	44.11	44.80	45.44	46.05
1.00E-01	39.29	39.62	40.03	40.80	41.54	42.24	42.91
1.50E-01	31.35	31.67	32.06	32.83	33.57	34.29	34.99
2.00E-01	26.08	26.35	26.68	27.34	27.98	28.61	29.23
2.23E-01	24.43	24.67	24.98	25.58	26.17	26.75	27.32
2.76E-01	21.92	22.12	22.37	22.87	23.36	23.85	24.34
2.84E-01	21.68	21.87	22.12	22.60	23.09	23.57	24.05
3.00E-01	21.17	21.36	21.59	22.05	22.52	22.97	23.43
3.03E-01	21.09	21.28	21.51	21.97	22.42	22.88	23.33
3.47E-01	20.10	20.27	20.47	20.88	21.29	21.70	22.11
3.56E-01	19.95	20.11	20.31	20.71	21.11	21.51	21.91
3.84E-01	19.53	19.68	19.87	20.24	20.62	21.00	21.38
4.00E-01	19.32	19.47	19.65	20.02	20.39	20.75	21.12
5.00E-01	18.48	18.60	18.76	19.08	19.40	19.72	20.04
6.00E-01	18.03	18.15	18.29	18.59	18.88	19.17	19.47
6.62E-01	17.85	17.97	18.10	18.39	18.67	18.95	19.24
8.00E-01	17.59	17.70	17.83	18.09	18.36	18.63	18.90
8.26E-01	17.56	17.66	17.79	18.05	18.32	18.59	18.85
1.00E+00	17.39	17.49	17.61	17.86	18.12	18.37	18.63
1.17E+00	17.29	17.39	17.51	17.76	18.01	18.26	18.51
1.33E+00	17.26	17.36	17.48	17.72	17.97	18.22	18.46
1.50E+00	17.27	17.37	17.49	17.73	17.98	18.22	18.47
2.00E+00	17.46	17.55	17.68	17.93	18.18	18.43	18.69
2.51E+00	17.78	17.88	18.01	18.27	18.53	18.80	19.06
3.00E+00	18.12	18.23	18.36	18.64	18.91	19.19	19.47
4.00E+00	18.87	18.99	19.14	19.44	19.74	20.04	20.35
5.00E+00	19.62	19.74	19.91	20.23	20.56	20.88	21.21
6.00E+00	20.30	20.44	20.61	20.96	21.30	21.65	22.00
8.00E+00	21.51	21.66	21.85	22.23	22.61	23.00	23.38
1.00E+01	22.50	22.66	22.87	23.28	23.69	24.10	24.51
1.50E+01	24.28	24.46	24.69	25.14	25.60	26.05	26.50

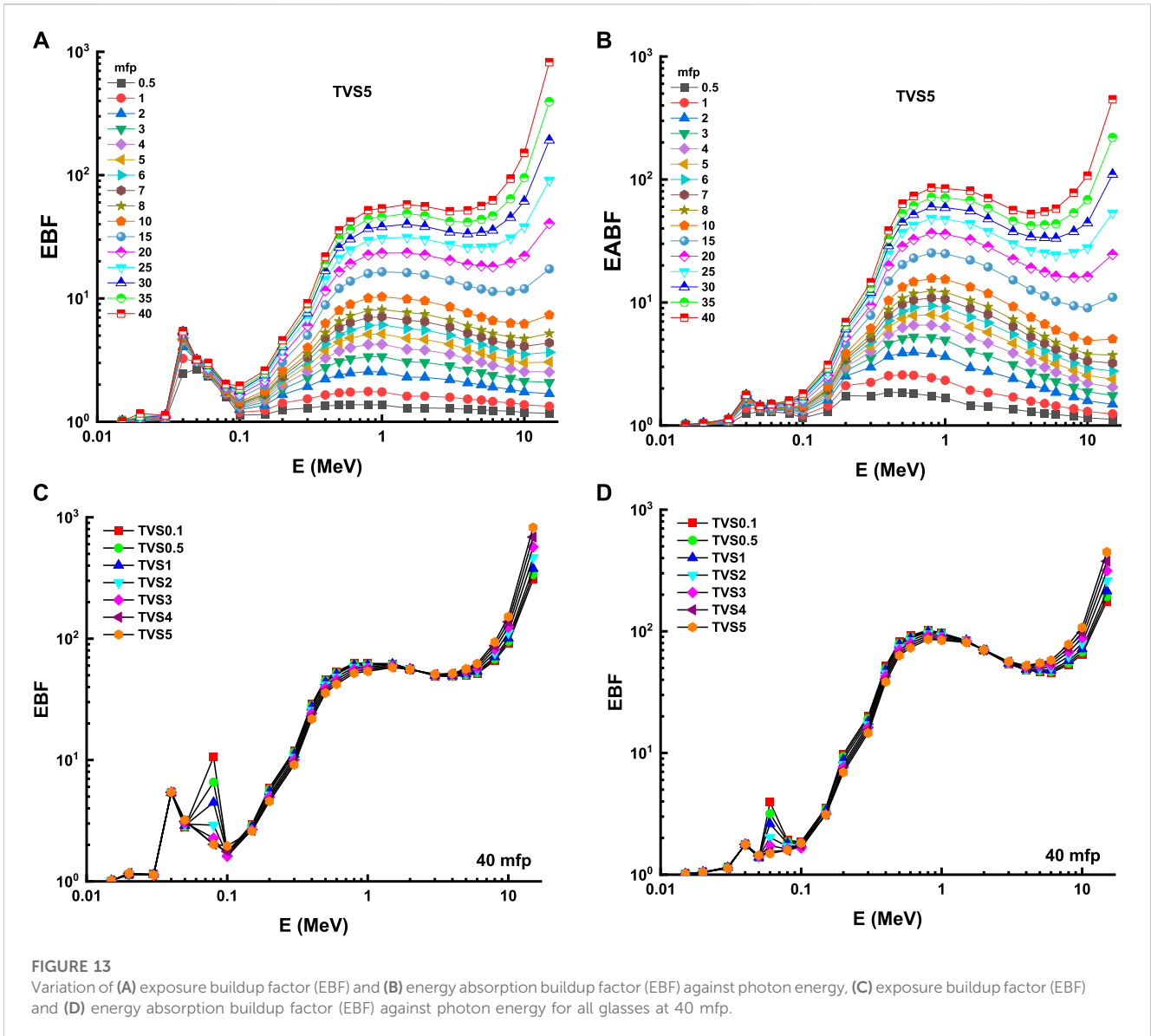


chance that photons will interact with the high-density sample because of how dense it is. Because of this, the number of photons that were able to go through the Glass was significantly decreased, which in turn resulted in a decrease in the G_{HVL} of the high-density Glass. In considering the fact that the TVS5 has the smallest G_{HVL} value of all of the glasses that were studied, it is compared with a number of typical photons shielding glasses and concretes, as shown in Figure 7, at 356, 662, 1173, and 1333 keV. The G_{HVL} value of the TVS5 glass material is shown to have a value, that is, lower than the G_{HVL} values of the various kinds of glass materials and concretes shown in these figures. It indicates that this particular glass sample has a higher capacity for absorption than S1 (Aktas et al., 2019), S2 (Yalcin et al., 2019), S3 (Mhareb et al., 2020), PCNKBi7.5 (Al-Yousef et al., 2021), Pb20 (Singh et al., 2014), PbG (Al-Harbi et al., 2021), S5 (Singh et al., 2022), (OC,

HSC, ILC, BMC, IC) concretes (Bashter, 1997). It has been shown that the Glass that was generated because of the ongoing study is more effective than other glasses and concretes when subjected to a certain photon energy. When these data are taken into consideration, it is feasible to reach the conclusion that TVS5 might be an alternative worth considering for usage as a material for radiation shielding.

3.4 The mean free path (G_{MFP})

In Figure 8; Table 4, the G_{MFP} was calculated based on the amount of Sm_2O_3 present in the sample. When it comes to radiation shielding technologies, a smaller G_{MFP} is preferred. As found in G_{HVL} , there is an inverse relationship between the G_{MFP} and the Sm_2O_3 concentration



(Abouhaswa et al., 2021). A lower G_{MFP} is the result of increasing the Sm_2O_3 concentration. Due to the addition of 5 mol% of Sm_2O_3 to the TVS0.1, TVS0.5, TVS1, TVS2, TVS3, TVS4, and TVS5 glasses, the G_{MFP} has been reduced from 1.978 to 1.760 cm at an energy of 356 keV. The finding demonstrates that when there is a higher concentration of Sm_2O_3 in the glasses as well as a higher density, the G_{MFP} decreases, and the glasses become better at shielding radiation.

3.5 The effective atomic number (Z_{eff})

In addition, we can talk about Z_{eff} . This is an important quantity, that is, often used in the field of radiation shielding to understand how efficient TVS0.1, TVS0.5, TVS1, TVS2, TVS3, TVS4, and TVS5 glasses are in obstructing the path of incoming photons (Kamisliloglu, 2021). Based on Z_{eff} we are in a position to form an opinion about the way in which the glasses react when they are subjected to gamma radiation. If a specific attenuator has a high Z_{eff} value, this suggests that it is superior to

other attenuators in terms of its ability to block the path of incoming photons (Lakshminarayana et al., 2020). The variation in Z_{eff} that takes place when the amount of energy is increased may be shown in Figure 9; Table 5 for the TVS0.1, TVS0.5, TVS1, TVS2, TVS3, TVS4, and TVS5 glasses. It is essential to take note that the Z_{eff} achieves its maximum value somewhere in the vicinity of 49.62 keV. Its value is 46.66 for TVS0.1, 46.93 for TVS0.5, 47.26 for TVS1, 47.88 for TVS2, 48.47 for TVS3, 49.01 for TVS4, and 49.52 for TVS5. In addition, we may infer from Figure 9; Table 5 that the incorporation of Sm_2O_3 increases the Z_{eff} values since these values are increased. Figure 9; Table 5 show that TVS5 has the greatest value for this parameter, while TVS0.1 has the lowest Z_{eff} value. We displayed the Z_{eff} for all TVS0.1, TVS0.5, TVS1, TVS2, TVS3, TVS4, and TVS5 glasses at 356 keV in order to demonstrate the accuracy of this discovery (Figure 9). When we go from TVS0.1 to TVS5, it is abundantly clear that the Z_{eff} is exhibiting an upward trend. According to these two data, the Glass with the composition of TVS5 is the most effective attenuator out of all the other glasses that were tested. Figure 10 shows the strong correlation between

Z_{eff} and effective electron density (N_{eff}). This figure observed that the TVS5 has the highest N_{eff} value at 356 keV. In addition, Figure 11 shows the correlation between the effective atomic number (Z_{eff}) and the density of glasses. While Figure 12 presents the correlation between (G_{MAC} , G_{HVL} , and G_{MFP}) and effective atomic number (Z_{eff}) of glasses. As seen in these figures, the Z_{eff} of glasses strongly correlated to the density of glasses, which affected G_{MAC} , G_{HVL} , and G_{MFP} .

3.6 Buildup factors

The nuclear photon build-up factor needs to be taken into consideration while gathering nuclear data for things like radiation shielding and dosimetry. The build-up factor is a measure of the proportion of the target, that is, contributed by photons that have collided. In this investigation, the geometry progressive (G-P) approach was used to calculate the values for the exposure build-up factor (EBF) and the energy absorption build-up factor (EABF) (Issa et al., 2017) (Supplementary Tables S1–S7). An earlier publication has all the material necessary to understand the G-P approach (Singh and Badiger, 2014). As a result, the relationship between the energy of the incoming photons and the variations in the EBF and EABF can be shown in Figure 13 for TVS0.1, TVS0.5, TVS1, TVS2, TVS3, TVS4, and TVS5 glass samples with penetration depths up to 40 mfp. The depth-dependent absorbance increases as the input energy lowers until it reaches its highest amount in the medium energy field, at which time it begins to fall. This continues till the depth-dependent absorption completely cancels out the medium energy field. Most of the gamma-ray absorption takes place in the lesser energy region, where PE predominates, and the high energy range, where PP predominates, both of which have little particle build-up. On the other hand, CS is the process, that is, seen the most often for photon-matter interaction at intermediate energies; yet it does not account for absolute photon loss. As a direct consequence of this, the EBF levels in the CS area are the highest (Sayyed et al., 2017). Apart from the fact that EBF levels might vary from area to region, it was discovered that the TVS5 sample had the lowest EBF values of all the samples that were analyzed (Figure 13C). The phrase energy absorption build-up factor (EABF) refers to the photon accumulation factor, with the quantity of interest being the energy, that is, absorbed or deposited in the material of interest. EABF values demonstrated a similar trend to EBF values. Because of this, the TVS5 sample also provided the lowest values for EABF (Figure 13D).

4 Conclusion

The XRD spectra of the produced samples demonstrate that the substances in question are amorphous. As more V_2O_5 was replaced with Sm_2O_3 , the average density values exhibited a tendency to rise, going from 4.367 to 4.598 g/cm³, demonstrating an increase in value. The radiation shielding characteristics are noticeably superior to those of a number of well-known and industry-standard radiation shielding glasses and materials. The study successfully applied the FLUKA Monte Carlo simulation in conjunction with the FLAIR graphical interface to determine the mass attenuation coefficients of glass compositions in the $65TeO_2-(35-x)V_2O_5-xSm_2O_3$ system. Our results showed that FLUKA simulation outcomes were in excellent agreement with theoretical calculations, validating the effectiveness of the FLUKA method for

mass attenuation coefficient determination. This study highlights the potential of the FLUKA Monte Carlo simulation as a reliable and accurate tool for addressing complex physics problems and supports its broader application in diverse research fields. Based on our comprehensive evaluation of its properties and performance, the TVS5 sample emerges as a highly effective material for radiation shielding industry, particularly the Glass with the greatest percentage of lead oxide concentration. Its superior gamma attenuation characteristics, coupled with an increased effective atomic number and electron density, indicate its significant potential in the field of radiation protection.

Data availability statement

The raw data supporting the conclusion of this article will be made available by the authors, without undue reservation.

Author contributions

Conceptualization, MU and SI; methodology, AM and AE; software, AM and HZ; validation, AA and MU; formal analysis, AA; investigation, MU; resources, AM and SI; data curation, AM, AE, and AA; writing—Original draft preparation, SI, and HZ; writing—Review and editing, MU, AB, HZ, and AE; visualization, AB, and AA; supervision, HZ; project administration, SI; The work of the author AE and APC was covered by “Dunarea de Jos” University of Galati, Romania. All authors contributed to the article and approved the submitted version.

Acknowledgments

This work was funded by the Dean of scientific Research at Jouf University under Grant Number (DSR2022-RG-0127).

Conflict of interest

The authors declare that the research was conducted in the absence of any commercial or financial relationships that could be construed as a potential conflict of interest.

Publisher's note

All claims expressed in this article are solely those of the authors and do not necessarily represent those of their affiliated organizations, or those of the publisher, the editors and the reviewers. Any product that may be evaluated in this article, or claim that may be made by its manufacturer, is not guaranteed or endorsed by the publisher.

Supplementary material

The Supplementary Material for this article can be found online at: <https://www.frontiersin.org/articles/10.3389/fmats.2023.1210524/full#supplementary-material>

References

- Abouhaswa, A. S., Zakaly, H. M. H., Issa, S. A. M., Rashad, M., Pyshkina, M., Tekin, H. O., et al. (2021). Synthesis, physical, optical, mechanical, and radiation attenuation properties of $\text{TiO}_2\text{-Na}_2\text{O-Bi}_2\text{O}_3\text{-B}_2\text{O}_3$ glasses. *Ceram. Int.* 47, 185–204. doi:10.1016/j.ceramint.2020.08.122
- Aktas, B., Yalcin, S., Dogru, K., Uzunoglu, Z., and Yilmaz, D. (2019). Structural and radiation shielding properties of chromium oxide doped borosilicate glass. *Radiat. Phys. Chem.* 156, 144–149. doi:10.1016/J.RADPHYS.2018.11.012
- Al-Hadeethi, Y., Al-Buriah, M. S., and Sayyed, M. I. (2020). Bioactive glasses and the impact of Si_3N_4 doping on the photon attenuation up to radiotherapy energies. *Ceram. Int.* 46, 5306–5314. doi:10.1016/j.ceramint.2019.10.281
- Al-Hadeethi, Y., and Sayyed, M. I. (2020). A comprehensive study on the effect of TeO_2 on the radiation shielding properties of $\text{TeO}_2\text{-B}_2\text{O}_3\text{-Bi}_2\text{O}_3\text{-LiF-SrCl}_2$ glass system using Phy-X/PSD software. *Ceram. Int.* 46, 6136–6140. doi:10.1016/j.ceramint.2019.11.078
- Al-Hadeethi, Y., and Sayyed, M. I. (2023). Correlation between the concentration of TeO_2 and the radiation shielding properties in the $\text{TeO}_2\text{-MoO}_3\text{-V}_2\text{O}_5$ glass system. *Nucl. Eng. Technol.* 55, 1218–1224. doi:10.1016/j.net.2022.12.014
- Al-Harbi, F. F., Prabhu, N. S., Sayyed, M. I., Almuqrin, A. H., Kumar, A., and Kamath, S. D. (2021). Evaluation of structural and gamma ray shielding competence of $\text{Li}_2\text{O-K}_2\text{O-B}_2\text{O}_3\text{-HMO (HMO = SrO/TeO}_2\text{/PbO/Bi}_2\text{O}_3)$ glass system. *Opt. (Stuttg.)* 248, 168074. doi:10.1016/J.IJLEO.2021.168074
- Al-Yousef, H. A., Sayyed, M. I., Alotiby, M., Kumar, A., Alghamdi, Y. S., Alotaibi, B. M., et al. (2021). Evaluation of optical, and radiation shielding features of New phosphate-based glass system. *Opt. (Stuttg.)* 242, 167220. doi:10.1016/J.IJLEO.2021.167220
- Almuqrin, A. H., Hanfi, M., Mahmoud, K. G., Sayyed, M. I., Al-Ghamdi, H., and Aloraini, D. A. (2021). The Role of La_2O_3 in Enhancement the radiation shielding efficiency of the tellurite glasses: Monte-Carlo simulation and theoretical study. *Mater. (Basel)* 14, 3913. doi:10.3390/ma14143913
- Aşkın, A. (2020). Gamma and neutron shielding characterizations of the $\text{Ag}_2\text{O-V}_2\text{O}_5\text{-MoO}_3\text{-TeO}_2$ quaternary tellurite glass system with the Geant4 simulation toolkit and Phy-X software. *Ceram. Int.* 46, 6046–6051. doi:10.1016/j.ceramint.2019.11.062
- Bagheri, R., Khorrami Moghaddam, A., and Yousefina, H. (2017). Gamma ray shielding study of barium-bismuth-borosilicate glasses as transparent shielding materials using MCNP-4C code, XCOM program, and available experimental data. *Nucl. Eng. Technol.* 49, 216–223. doi:10.1016/j.net.2016.08.013
- Bashter, I. I. (1997). Calculation of radiation attenuation coefficients for shielding concretes. *Ann. Nucl. Energy* 24, 1389–1401. doi:10.1016/S0306-4549(97)00003-0
- Battistoni, G., Cerutti, F., Fassò, A., Ferrari, A., Muraro, S., Ranft, J., et al. (2007). The FLUKA code: Description and benchmarking. *AIP Conf. Proc. (AIP)*, 31–49. doi:10.1063/1.2720455
- Biswas, J., Jana, S., Ghosh, S., and Mahalingam, V. (2022). Optical and luminescence properties of Sm_2O_3 doped $\text{SrO-PbO-ZnO-P}_2\text{O}_5\text{-TeO}_2$ glasses for visible laser applications. *Solid State Sci.* 129, 106910. doi:10.1016/j.solidstatesciences.2022.106910
- Çelikbilek, M., Erçin Ersundu, A., and Aydin, S. (2013). Glass formation and characterization studies in the $\text{TeO}_2\text{-WO}_3\text{-Na}_2\text{O}$ system. *J. Am. Ceram. Soc.* 96, 1470–1476. doi:10.1111/jace.12335
- Divina, R., Marimuthu, K., Sayyed, M. I., Tekin, H. O., and Agar, O. (2019). Physical, structural, and radiation shielding properties of $\text{B}_2\text{O}_3\text{-MgO-K}_2\text{O-Sm}_2\text{O}_3$ glass network modified with TeO_2 . *Radiat. Phys. Chem.* 160, 75–82. doi:10.1016/j.radphyschem.2019.03.029
- D'Souza, A. N., Prabhu, N. S., Sharmila, K., Sayyed, M. I., Somshekarappa, H. M., Lakshminarayana, G., et al. (2020). Role of Bi_2O_3 in altering the structural, optical, mechanical, radiation shielding and thermoluminescence properties of heavy metal oxide borosilicate glasses. *J. Non. Cryst. Solids* 542, 120136. doi:10.1016/j.jnoncrysol.2020.120136
- El-Denglawey, A., Zakaly, H. M. H., Alshammari, K., Issa, S. A. M., Tekin, H. O., AbuShanab, W. S., et al. (2021). Prediction of mechanical and radiation parameters of glasses with high Bi_2O_3 concentration. *Results Phys.* 21, 103839. doi:10.1016/j.rinp.2021.103839
- El-Taher, A., Zakaly, H. M. H., Pyshkina, M., Allam, E. A., El-Sharkawy, R. M., Mahmoud, M. E., et al. (2021). A comparative study between Fluka and Microshield Modeling calculations to study the radiation-shielding of nanoparticles and Plastic waste composites. *Z. fur Anorg. Allg. Chem.* 647, 1083–1090. doi:10.1002/zaac.202100062
- Elazaka, A. I., Zakaly, H. M. H., Issa, S. A. M., Rashad, M., Tekin, H. O., Saudi, H. A., et al. (2021). New approach to removal of hazardous Bypass Cement Dust (BCD) from the environment: $20\text{Na}_2\text{O-}20\text{BaCl}_2\text{(}60\text{-x)B}_2\text{O}_3\text{(x)BCD}$ glass system and optical, mechanical, structural and nuclear radiation shielding competences. *J. Hazard. Mater.* 403, 123738. doi:10.1016/j.jhazmat.2020.123738
- Ferrari, A., Sala, P. R., Fassò, A., and Ranft, J. (2005). *Fluka: A Multi-particle Transport code*. CERN-2005-10, INFN/TC 05/11, SLAC-R-773. doi:10.2172/877507
- Gaikwad, D. K., Sayyed, M. I., Obaid, S. S., Issa, S. A. M., and Pawar, P. P. (2018). Gamma ray shielding properties of $\text{TeO}_2\text{-ZnF}_2\text{-As}_2\text{O}_3\text{-Sm}_2\text{O}_3$ glasses. *J. Alloys Compd.* 765, 451–458. doi:10.1016/j.jallcom.2018.06.240
- Hussey, N. E., MacNeil, M. A., Olin, J. A., McMeans, B. C., Kinney, M. J., Chapman, D. D., et al. (2012). Stable isotopes and elasmobranchs: Tissue types, methods, applications and assumptions. *J. Fish. Biol.* 80, 1449–1484. doi:10.1111/j.1095-8649.2012.03251.x
- Ibrahim, S. E., Rammah, Y. S., Hager, I. Z., and El-Mallawany, R. (2018). UV and electrical properties of $\text{TeO}_2\text{-WO}_3\text{-Li}_2\text{O-Nb}_2\text{O}_5\text{/Sm}_2\text{O}_3\text{/Pr}_6\text{O}_{11}\text{/Er}_2\text{O}_3$ glasses. *J. Non. Cryst. Solids* 498, 443–447. doi:10.1016/j.jnoncrysol.2018.02.019
- Ilik, E., Kavaz, E., Kilic, G., Issa, S. A. M., Zakaly, H. M. H., and Tekin, H. O. (2022). A closer-look on Copper(II) oxide reinforced Calcium-Borate glasses: Fabrication and multiple experimental assessment on optical, structural, physical, and experimental neutron/gamma shielding properties. *Ceram. Int.* 48, 6780–6791. doi:10.1016/j.ceramint.2021.11.229
- Issa, S. A. M., Ali, A. M., Tekin, H. O., Saddeek, Y. B., Al-Hajry, A., Algarni, H., et al. (2020). Enhancement of nuclear radiation shielding and mechanical properties of YBiO_3 glasses using La_2O_3 . *Nucl. Eng. Technol.* 52, 1297–1303. doi:10.1016/j.net.2019.11.017
- Issa, S. A. M., Darwish, A. A. A., and El-Nahass, M. M. (2017). The evolution of gamma-rays sensing properties of pure and doped phthalocyanine. *Prog. Nucl. Energy* 100, 276–282. doi:10.1016/J.PNUCENE.2017.06.016
- Issa, S. A. M., and Mostafa, A. M. A. (2017). Effect of Bi_2O_3 in borate-tellurite-silicate glass system for development of gamma-rays shielding materials. *J. Alloys Compd.* 695, 302–310. doi:10.1016/j.jallcom.2016.10.207
- Kamisliloglu, M. (2021). Research on the effects of bismuth borate glass system on nuclear radiation shielding parameters. *Results Phys.* 22, 103844. doi:10.1016/j.rinp.2021.103844
- Kilic, G., Ilik, E., Issa, S. A. M., Issa, B., Issever, U. G., Zakaly, H. M. H., et al. (2021). Fabrication, structural, optical, physical and radiation shielding characterization of indium (III) oxide reinforced $85\text{TeO}_2\text{(}15\text{-x)ZnO-xIn}_2\text{O}_3$ glass system. *Ceram. Int.* 47, 27305–27315. doi:10.1016/j.ceramint.2021.06.152
- Kilic, G., Issa, S. A. M., Ilik, E., Kilicoglu, O., and Tekin, H. O. (2020). A journey for exploration of Eu_2O_3 reinforcement effect on zinc-borate glasses: Synthesis, optical, physical and nuclear radiation shielding properties. *Ceram. Int.* 47, 2572–2583. doi:10.1016/j.ceramint.2020.09.103
- Ladenson, P. W., Braverman, L. E., Mazzaferri, E. L., Brucker-Davis, F., Cooper, D. S., Garber, J. R., et al. (1997). Comparison of administration of Recombinant human Thyrotropin with Withdrawal of thyroid Hormone for radioactive Iodine scanning in Patients with thyroid Carcinoma. *N. Engl. J. Med.* 337, 888–896. doi:10.1056/NEJM199709253371304
- Lakshminarayana, G., Kumar, A., Tekin, H. O., Issa, S. A. M., Al-Buriah, M. S., Lee, D. E., et al. (2020). Binary $\text{B}_2\text{O}_3\text{-Bi}_2\text{O}_3$ glasses: Scrutinization of directly and indirectly ionizing radiations shielding abilities. *J. Mater. Res. Technol.* 9, 14549–14567. doi:10.1016/j.jmrt.2020.10.019
- Madbouly, A. M., Sallam, O. I., Issa, S. A. M., Rashad, M., Hamdy, A., Tekin, H. O., et al. (2022). Experimental and FLUKA evaluation on structure and optical properties and γ -radiation shielding capacity of bismuth borophosphate glasses. *Prog. Nucl. Energy* 148, 104219. doi:10.1016/J.PNUCENE.2022.104219
- Mahmoud, I. S., Issa, S. A. M., Zakaly, H. M. H., Saudi, H. A., Ali, A. S., Saddeek, Y. B., et al. (2021). Material characterization of $\text{WO}_3/\text{Bi}_2\text{O}_3$ substituted calcium-borosilicate glasses: Structural, physical, mechanical properties and gamma-ray resistance competencies. *J. Alloys Compd.* 888, 161419. doi:10.1016/j.jallcom.2021.161419
- Mark, S., Khomchenko, S., Shifrin, M., Haviv, Y., Schwartz, J. R., and Orion, I. (2007). TVF-NMCRC-A powerful program for writing and executing simulation inputs for the Fluka Monte Carlo Code system. *Nucl. Instrum. Methods Phys. Res. Sect. A Accel. Spectrom. Detect. Assoc. Equip.* 572, 929–934. doi:10.1016/j.nima.2006.12.007
- Mhareb, M. H. A., Alajerami, Y. S. M., Sayyed, M. I., Dwaikat, N., Alqahtani, M., Alshahri, F., et al. (2020). Radiation shielding, structural, physical, and optical properties for a series of borosilicate glass. *J. Non. Cryst. Solids* 550, 120360. doi:10.1016/J.JNONCRYSol.2020.120360
- Miousse, I. R., Kutanz, K. R., and Koturbash, I. (2017). Effects of ionizing radiation on DNA methylation: From experimental biology to clinical applications. *Int. J. Radiat. Biol.* 93, 457–469. doi:10.1080/09553002.2017.1287454
- Mostafa, A. M. A., Issa, S. A. M., Zakaly, H. M. H., Zaid, M. H. M., Tekin, H. O., Matori, K. A., et al. (2020a). The influence of heavy elements on the ionizing radiation shielding efficiency and elastic properties of some tellurite glasses: Theoretical investigation. *Results Phys.* 19, 103496. doi:10.1016/j.rinp.2020.103496
- Mostafa, A. M. A., Zakaly, H. M. H., Pyshkina, M., Issa, S. A. M., Tekin, H. O., Sidek, H. A. A., et al. (2020b). Multi-objective optimization strategies for radiation shielding performance of BZBB glasses using Bi_2O_3 : A FLUKA Monte Carlo code calculations. *J. Mater. Res. Technol.* 9, 12335–12345. doi:10.1016/J.JMRT.2020.08.077
- Rammah, Y. S., Al-Buriah, M. S., and Abouhaswa, A. S. (2020). $\text{B}_2\text{O}_3\text{-BaCO}_3\text{-Li}_2\text{O}_3$ glass system doped with Co_3O_4 : Structure, optical, and

- radiation shielding properties. *Phys. B Condens. Matter* 576, 411717. doi:10.1016/J.PHYSB.2019.411717
- Rashad, M., Tekin, H. O., Zakaly, H. M., Pyshkina, M., Issa, S. A. M., and Susoy, G. (2020). Physical and nuclear shielding properties of newly synthesized magnesium oxide and zinc oxide nanoparticles. *Nucl. Eng. Technol.* 52, 2078–2084. doi:10.1016/j.net.2020.02.013
- Sadeq, M. S., Bashter, I. I., Salem, S. M., Mansour, S. F., Saudi, H. A., Sayyed, M. I., et al. (2022). Enhancing the gamma-ray attenuation parameters of mixed bismuth/barium borosilicate glasses: Using an experimental method, Geant4 code and XCOM software. *Prog. Nucl. Energy* 145, 104124. doi:10.1016/j.pnucene.2022.104124
- Şakar, E., Özpolat, Ö. F., Alim, B., Sayyed, M. I., and Kurudirek, M. (2020). Phy-X/PSD: Development of a user friendly online software for calculation of parameters relevant to radiation shielding and dosimetry. *Radiat. Phys. Chem.* 166, 108496. doi:10.1016/J.RADPHYSICHEM.2019.108496
- Saudi, H. A., Tekin, H. O., Zakaly, H. M. H., Issa, S. A. M., Susoy, G., and Zhukovsky, M. (2021). The impact of samarium (III) oxide on structural, optical and radiation shielding properties of thallium-borate glasses: Experimental and numerical investigation. *Opt. Mater. (Amst.)* 114, 110948. doi:10.1016/j.optmat.2021.110948
- Sayyed, M. I., Issa, S. A. M., and Auda, S. H. (2017). Assessment of radio-protective properties of some anti-inflammatory drugs. *Prog. Nucl. Energy* 100, 297–308. doi:10.1016/j.pnucene.2017.07.003
- Schellekens, R. C. A., Stellaard, F., Woerdenbag, H. J., Frijlink, H. W., and Kosterink, J. G. W. (2011). Applications of stable isotopes in clinical pharmacology. *Br. J. Clin. Pharmacol.* 72, 879–897. doi:10.1111/j.1365-2125.2011.04071.x
- Selvi, S., Marimuthu, K., and Muralidharan, G. (2017). Effect of PbO on the B 2 O 3 -TeO 2 -P 2 O 5 -BaO-CdO-Sm 2 O 3 glasses - structural and optical investigations. *J. Non. Cryst. Solids* 461, 35–46. doi:10.1016/j.jnoncrsol.2017.01.028
- Sidkey, M. A., Abd El-Moneim, A., and Abd El-Latif, L. (1999). Ultrasonic studies on ternary TeO₂-V₂O₅-Sm₂O₃ glasses. *Mater. Chem. Phys.* 61, 103–109. doi:10.1016/S0254-0584(99)00067-X
- Singh, K. J., Kaur, S., and Kaundal, R. S. (2014). Comparative study of gamma ray shielding and some properties of PbO-SiO₂-Al₂O₃ and Bi₂O₃-SiO₂-Al₂O₃ glass systems. *Radiat. Phys. Chem.* 96, 153–157. doi:10.1016/j.radphyschem.2013.09.015
- Singh, S., Kaur, R., Rani, S., and Sidhu, B. S. (2022). Physical, structural and nuclear radiation shielding behaviour of xBaO-(0.30-x)MgO-0.10Na₂O-0.10Al₂O₃-0.50B₂O₃ glass matrix. *Mater. Chem. Phys.* 276, 125415. doi:10.1016/j.matchemphys.2021.125415
- Singh, V. P., and Badiger, N. M. (2014). Energy absorption buildup factors, exposure buildup factors and Kerma for optically stimulated luminescence materials and their tissue equivalence for radiation dosimetry. *Radiat. Phys. Chem.* 104, 61–67. doi:10.1016/j.radphyschem.2013.11.025
- Susoy, G., Guclu, E. E. A., Kilicoglu, O., Kamislioglu, M., Al-Buriah, M. S., Abuzaid, M. M., et al. (2020). The impact of Cr₂O₃ additive on nuclear radiation shielding properties of LiF-SrO-B₂O₃ glass system. *Mater. Chem. Phys.* 242, 122481. doi:10.1016/j.matchemphys.2019.122481
- Turky, G., and Dawy, M. (2003). Spectral and electrical properties of ternary (TeO₂-V₂O₅-Sm₂O₃) glasses. *Mater. Chem. Phys.* 77, 48–59. doi:10.1016/S0254-0584(01)00574-0
- Yalcin, S., Aktas, B., and Yilmaz, D. (2019). Radiation shielding properties of Cerium oxide and Erbium oxide doped obsidian glass. *Radiat. Phys. Chem.* 160, 83–88. doi:10.1016/J.RADPHYSICHEM.2019.03.024
- Zakaly, H. M. H., Issa, S. A. M., Tekin, H. O., Badawi, A., Saudi, H. A., Henaish, A. M. A., et al. (2022). An experimental evaluation of CdO/PbO-B₂O₃ glasses containing neodymium oxide: Structure, electrical conductivity, and gamma-ray resistance. *Mater. Res. Bull.* 151, 111828. doi:10.1016/j.materresbull.2022.111828
- Zakaly, H. M. H., Saudi, H. A., Issa, S. A. M., Rashad, M., Elazaka, A. I., Tekin, H. O., et al. (2021a). Alteration of optical, structural, mechanical durability and nuclear radiation attenuation properties of barium borosilicate glasses through BaO reinforcement: Experimental and numerical analyses. *Ceram. Int.* 47, 5587–5596. doi:10.1016/j.ceramint.2020.10.143
- Zakaly, H. M. H., Saudi, H. A., Tekin, H. O., Rashad, M., Issa, S. A. M., Rammah, Y. S., et al. (2021b). Glass fabrication using ceramic and porcelain recycled waste and lithium niobate: Physical, structural, optical and nuclear radiation attenuation properties. *J. Mater. Res. Technol.* 15, 4074–4085. doi:10.1016/J.JMRT.2021.09.138
- Zhukovsky, M., Koubisy, M. S. I., Zakaly, H. M. H., Ali, A. S., Issa, S. A. M., and Tekin, H. O. (2022). Dielectric, structural, optical and radiation shielding properties of newly synthesized CaO-SiO₂-Na₂O-Al₂O₃ glasses: Experimental and theoretical investigations on impact of Tungsten(III) oxide. *Appl. Phys. A* 128, 205. doi:10.1007/s00339-022-05328-z